Video Article

Using Retinal Imaging to Study Dementia

Victor T.T. Chan[1], Tiffany H.K. Tso[1], Fangyao Tang[1], Clement Tham[1], Vincent Mok[2,3,4], Christopher Chen[5,6], Tien Y. Wong[7,8], Carol Y. Cheung[1]

[1]Department of Ophthalmology and Visual Sciences, The Chinese University of Hong Kong

[2]Department of Medicine & Therapeutics, The Chinese University of Hong Kong

[3]Therese Pei Fong Chow Research Centre for Prevention of Dementia, The Chinese University of Hong Kong

[4]Gerald Choa Neuroscience Centre, The Chinese University of Hong Kong

[5]Memory Aging and Cognition Centre, National University Health System

[6]Department of Pharmacology, National University of Singapore

[7]Singapore Eye Research Institute, Singapore National Eye Centre

[8]Duke-NUS Medical School, National University of Singapore

Correspondence to: Carol Y. Cheung at carolcheung@cuhk.edu.hk

URL: https://www.jove.com/video/56137
DOI: doi:10.3791/56137

Keywords: Medicine, Issue 129, Retinal imaging, Dementia, Alzheimer's Disease, Optical Coherence Tomography, Fundus Photography, Retinal microvasculature, Small vessel disease, Retinal Nerve Fiber Layer, Ganglion Cell-Inner Plexiform Layer

Date Published: 11/6/2017

Citation: Chan, V.T., Tso, T.H., Tang, F., Tham, C., Mok, V., Chen, C., Wong, T.Y., Cheung, C.Y. Using Retinal Imaging to Study Dementia. *J. Vis. Exp.* (129), e56137, doi:10.3791/56137 (2017).

Abstract

The retina offers a unique “window” to study pathophysiological processes of dementia in the brain, as it is an extension of the central nervous system (CNS) and shares prominent similarities with the brain in terms of embryological origin, anatomical features and physiological properties. The vascular and neuronal structure in the retina can now be visualized easily and non-invasively using retinal imaging techniques, including fundus photography and optical coherence tomography (OCT), and quantified semi-automatically using computer-assisted analysis programs. Studying the associations between vascular and neuronal changes in the retina and dementia could improve our understanding of dementia and, potentially, aid in diagnosis and risk assessment. This protocol aims to describe a method of quantifying and analyzing retinal vasculature and neuronal structure, which are potentially associated with dementia. This protocol also provides examples of retinal changes in subjects with dementia, and discusses technical issues and current limitations of retinal imaging.

Video Link

The video component of this article can be found at https://www.jove.com/video/56137/

Introduction

Owing to increases in life expectancy, dementia has become a major medical problem, contributing to significant social and economic health burden globally[1,2,3,4,5]. Today, a person in the United States develops Alzheimer’s Disease (AD), the most common form of dementia, every 66 s[6]. It has been estimated that by the year 2050, 115 million people will be affected by AD[7].

The retina offers a unique “window” to study dementia due to its similar anatomical and physiological properties with the brain. In terms of vasculature, the retinal arterioles and venules, measuring 100 to 300 µm in diameter, share similar features with cerebral small vessels, such as end arterioles without anastomoses, barrier function, and auto-regulation[8,9]. In terms of neuronal structure, retinal ganglionic cells (RGCs) share typical properties with neurons in the central nervous system (CNS)10. The RGCs are prominently connected with the brain as they form the optic nerve and project visual signals from the retina to the lateral geniculate nuclei and the superior colliculus. The optic nerve, similar to many neuronal fibers in the CNS, is myelinated by oligodendrocytes and is ensheathed in meningeal layers. Notably, an insult to the optic nerve can result in similar responses observed in other CNS axons, such as retrograde and anterograde degeneration of the axon, scar formation, myelin destruction, secondary degeneration, and an abnormal level of neurotrophic factors and neurotransmitters[11,12,13,14]. The appearance of visual symptoms in some AD patients may also be explained by the robust associations between the retina and the brain[15,16]. As a result, it has been suggested that the retina may reflect the pathological processes of dementia in the brain and retinal imaging can be used to study dementia.

The retinal vasculature and neuronal structure can now be visualized non-invasively using retinal imaging techniques. For instance, retinal fundus photographs can be captured using fundus cameras, and characteristics of the retinal vasculature (*e.g.,* vessel caliber, tortuosity, and fractal dimension) can then be quantified using computer-assisted analysis programs. In addition, parameters of the retinal neuronal structure (such as the thickness of ganglion cell-inner plexiform layer [GC-IPL] and retinal nerve fiber layer [RNFL]) can also be measured using optic coherence tomography (OCT) and quantified using the built-in analysis algorithms.

In view of the importance of retinal imaging to studying dementia, this protocol aims to describe a method of imaging and analyzing retinal vasculature and neuronal structure *in vivo* using retinal imaging techniques. This protocol also provides examples of retinal changes in subjects with dementia, and discusses technical issues and current limitations of retinal imaging.

Protocol

All methods described here have been approved by a local clinical research ethics committee in Hong Kong.

Note: For simplicity, the equipment listed in the **Table of Materials** is used to illustrate the procedures of retinal imaging and subsequent analysis. Measurement of retinal vascular parameters is illustrated using the Singapore I Vessel Assessment program (SIVA) [17] (Version 4.0, National University of Singapore, Singapore). However, it should be noted that a different set of equipment can be adopted as the underlying principles remain similar.

1. Prepare the Subjects for Retinal Imaging

1. Dilate the subjects' pupils using a mydriatic agent. Wait for at least 15 min to establish sufficient pupil dilation.

2. Measure Retinal Vascular Parameters from Fundus Photographs Using a Computer-assisted Analysis program

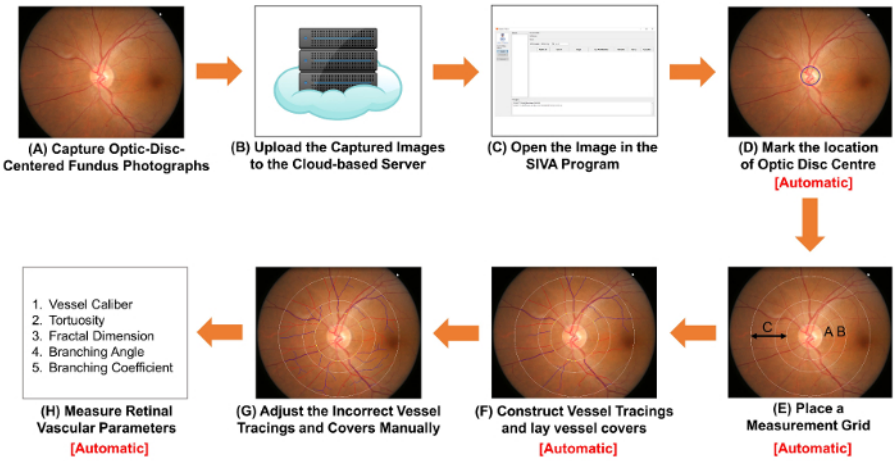

Figure 1: Schematic diagram showing the procedures of measuring retinal vascular parameters. (**A**) Obtain optic-disc-centered fundus photographs using a fundus camera. **Figure 1A** and **Figure 2A** are two fundus photographs with optimal quality. (**B**) Upload the fundus photographs to the cloud-based server and enter relevant study details, including the image conversion factor (ICF). Other computer-assisted analysis programs may use non-cloud-based methods to organize and store the images. (**C**) Open the fundus photograph in the computer-assisted analysis program. (**D**) Mark the location of optic disc center, and (**E**) prompt the software to automatically detect the rim of optic disc and place a measurement grid. (**F**) Construct vessel tracings based on the vessel paths, and lay vessel covers to estimate the diameters of the vessels. (**G**) Adjust the incorrect vessel tracings and vessel covers manually. (**H**) Measure a spectrum of retinal vascular parameters, including vessel calibers, tortuosity, fractal dimension and bifurcation. Step (**D**) to Step (**F**), and Step (**H**) can be automatically performed by some computer-assisted analysis programs. Please click here to view a larger version of this figure.

1. **Capture fundus photographs using a fundus camera.**
    1. Turn on the fundus camera and launch the image capturing program on the computer. Rest the chin of the subject properly on the chinrest with the forehead against the head strap. Move the control lever to align the light beam properly to the subject's pupil.
    2. Align the illumination points until both appear smallest on both sides in the viewfinder. Move the external fixation target to guide the subject's eyes until the optic disc is at the center of the viewfinder and the regions of interest (ROI) are well within the boundaries. Adjust the focusing knob to focus on the retina.
    3. Have the subject firmly look at the external fixation target and ensure the subject's eyes are not filled with tears.
    4. Depress the shutter-release button to capture an image (**Figure 1A**).
    5. Check the quality of the fundus photograph captured, using **Figure 2A** as a standard. Discard the image and repeat the image acquisition process (i.e., Step 2.1.1 to 2.1.4) if the pupil is poorly dilated (**Figure 2B**), the optic disc is not at the center of the image (**Figure 2C**), or the image is out of focus (**Figure 2D**).
    6. Save the image in TIFF format with gradable resolution (*i.e.*, approximately 3,000 pixels x 2,000 pixels, at more than 150 dpi).
    Note: The protocol can be paused here.
    7. Repeat Steps 2.1.1 to 2.1.6 to acquire fundus photographs for other subjects.
    8. Select a 10% sample of images randomly and measure the height of optic discs in these images (**Figure 3**). Calculate the image conversion factor (ICF) using the formula:
    ICF = 1,800 µm/(Average pixel height of optic discs of the images sampled).

9. Upload the captured fundus photographs to the cloud-based server and enter relevant study details, including the image conversion factor (ICF) (**Figure 1B**).
   Note: The protocol can be paused here. Other computer-assisted analysis programs may use other non-cloud-based methods to organize the images and record the ICF.

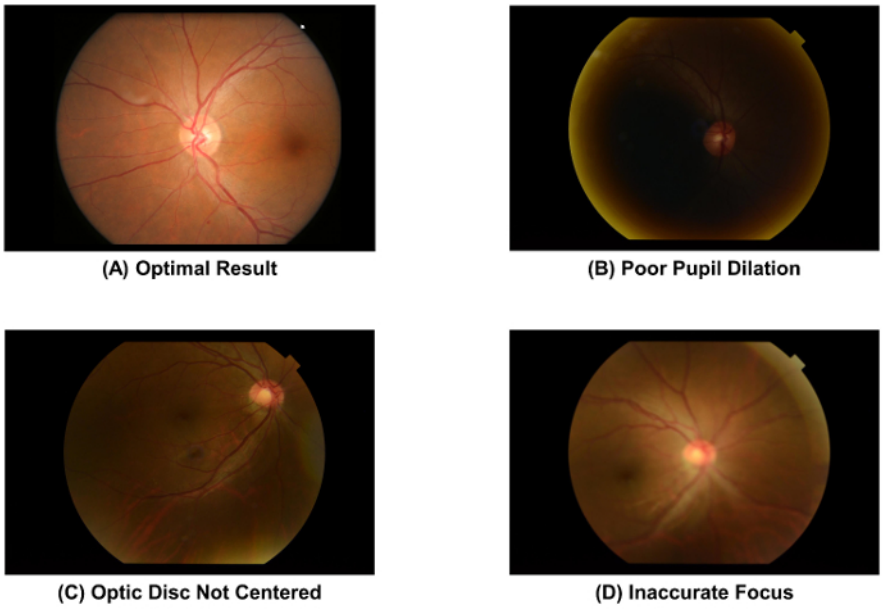

Figure 2: Fundus photographs with optimal and suboptimal quality. The image quality of a fundus photograph must be checked immediately after image acquisition, as the image quality directly affects the subsequent measurement of retinal vascular parameters. The image should be discarded if one of these artefacts is observed. These images were captured using a 50° fundus camera. Please click here to view a larger version of this figure.

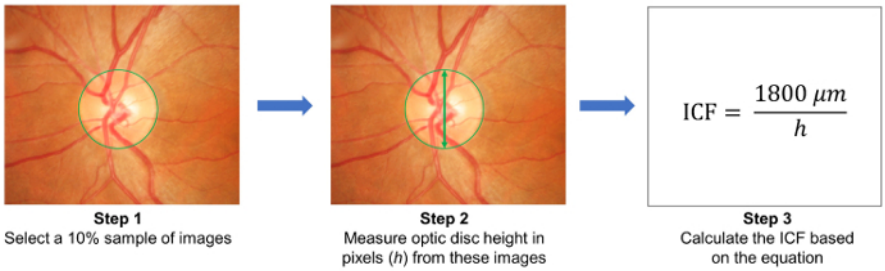

Figure 3: Calculation of the image conversion factor (ICF). To calculate the ICF, randomly select a 10% sample of images from the study (Step 1). Then, measure the height of optic discs (in pixels) from the images sampled (Step 2). Calculate the ICF using the formula: ICF= 1800 µm / (Average pixel height of optic discs of the sampled images), where 1800 µm is approximately the height of a normal optic disc (Step 3). As magnification effect and image resolution differ from camera to camera, it is necessary to calculate an accurate ICF for each camera used. Please click here to view a larger version of this figure.

2. **Open the fundus photograph in a computer-assisted analysis program. Construct vessel tracings and lay vessel covers for the retinal vasculature.**
   Note: In this section, the SIVA program is used to illustrate the procedures. However, the SIVA program can be substituted by other available computer-assisted analysis programs. In addition, Steps 2.2.2 to 2.2.3 are automatically performed by some computer-assisted analysis programs when a fundus photograph is opened (*i.e.* Step 2.2.1).
   1. Open the fundus photograph with the computer-assisted analysis program (**Figure 1C**).
   2. Mark the location of the optic disc centre (**Figure 1D**).
      1. Click the “OD Center” button on the left function panel; the mouse cursor will be replaced by a green circle.
      2. Move the green circle to the center of the optic disc (OD), and left-click to fix the circle.
      3. Prompt the software to automatically place a measurement grid, construct vessel tracings and lay vessel covers (**Figure 1E** and **1F**).
         Note: Vessel covers are measurement lines that estimate the approximate width of the internal lumens of the vessels.
         1. Click the “Find OD” button to prompt the software to detect the OD rim and place four concentric circles as a measurement grid, based on the position of the OD center.
         2. Click the “Process” button to initiate the automatic vessel tracing process.

3. **Adjust incorrect vessel tracings manually. Begin the inspection from the 12 o'clock position in a clockwise manner to ensure that all vessel tracings are verified.**
    1. Check that the optic disc is accurately detected and the measurement grid is correctly placed. Adjust the measurement grid manually following steps 2.2.2 to 2.2.3, if the innermost circle does not accurately outline the optic disc rim (**Figure 4A**).
    2. Left click to select vessel tracing(s) labelled with incorrect vessel type (arterioles versus venules) and click the "Vessel (T)ype" button to change the vessel type.
    Note: Arterioles are labelled in red and venules are labelled in blue. Arterioles can be distinguished from venules based on their physiological differences. For example, venules are generally darker in color and wider than arterioles. Vessels with same vessel type usually do not cross each other.
    3. Extend incomplete vessel tracings following steps 2.3.3.1 to 2.3.3.2 (**Figure 4B**).
        1. Use the cursor to click at the distal end of the incomplete vessel tracing. Left click at points along the vessel path to extend the vessel tracing.
        2. Stop the tracing process when the distal end of the vessel is reached. Stop the tracing at the outermost white circle if the distal part of the vessel falls outside the measurement grid (see **Figure 4B**).
    4. Adjust vessel tracings if the vessel paths are not traced correctly at the crossover site (**Figure 4C**).
        1. Click the "Select" button and then click at the incorrect point of the vessel tracing. Click the "Brea(k) Seg" button to disconnect the vessel tracing at the point selected. Select the disconnected segment and click the "(Del) Seg" button to delete it.
        2. Re-construct a new vessel tracing using steps 2.3.3.1 and 2.3.3.2.

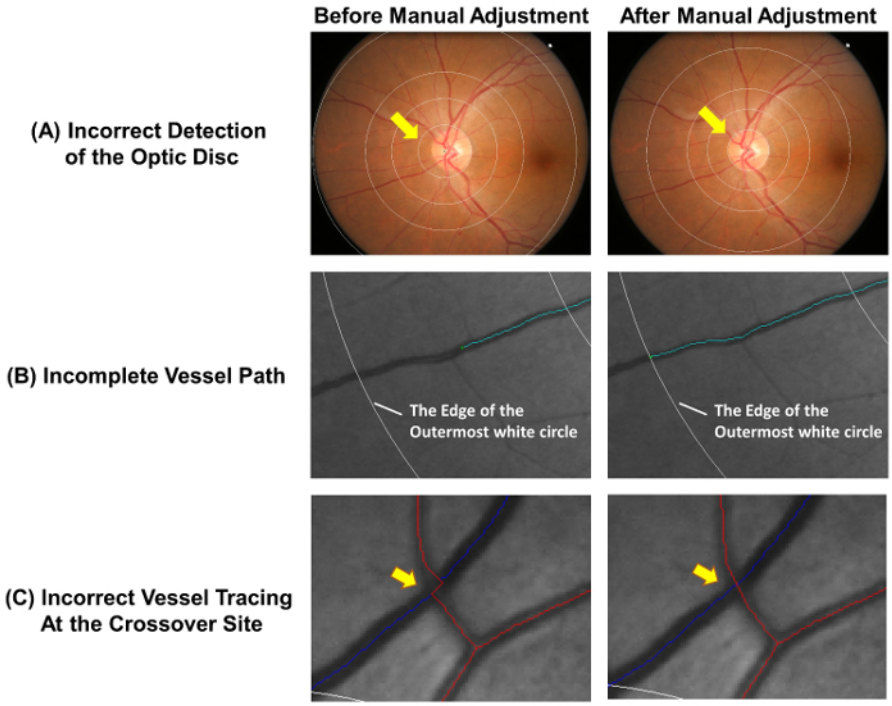

Figure 4: Common errors of the auto-tracing. The automatic vessel tracing is not completely accurate and manual adjustments are required to ensure the accuracy of measurement. This figure shows common errors of the auto-tracing and demonstrates optimal results after manual adjustments. (**A**) The optic disc center is incorrectly marked and this lead to deviation of the measurement grid, which may affect the subsequent measurements. Ideally, the innermost circle of the measurement grid should outline the optic disc rim. (**B**) Incomplete vessel tracing could lead to the incorrect measurement of fractal dimension, tortuosity, *etc.* The vessel path should be traced until the end of the vessel. If the distal part of the vessel falls outside the measurement grid, the tracing can be stopped at the outermost white circle. (**C**) Vessel tracings at the crossover sites are subject to a higher tendency of error and thus require special attention. Please click here to view a larger version of this figure.

4. **Lay vessel covers on all vessel segments and deactivate the incorrect covers manually.**
    1. Click the "Find Covers" button to lay vessel covers on all vessel segments automatically.
    2. Check if all vessel covers are correctly placed. Left-click and drag the cursor to deactivate vessel covers if the covers are not laid perpendicular to the vessel walls (**Figure 5A**), the vessel path is obscured by another vessel (**Figure 5B**), or the covers overestimate or underestimate the width of the vessel lumen (**Figure 5C**).

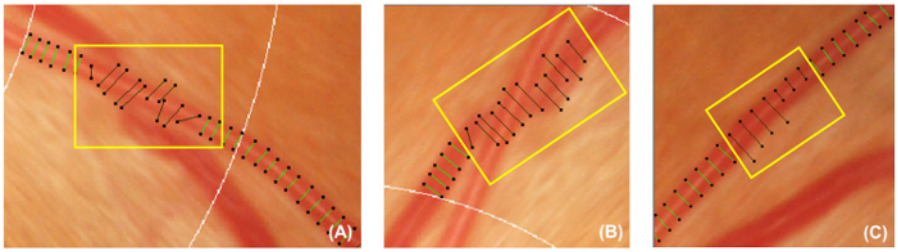

Figure 5: Incorrect vessel covers. This figure shows examples of incorrect vessel covers that should be deactivated and excluded from the subsequent measurement. Vessel covers should be deactivated if they are not perpendicular to the vessels (**A**). In addition, Vessel covers should also be deactivated if the vessel being traced is obscured under another vessel (**B**), or the vessel covers cannot represent the approximate width of the vessel (**C**). Please click here to view a larger version of this figure.

5. **Measure retinal vascular parameters from the vessel tracings and the vessel covers**
   Note: Step 2.5 is performed automatically by a computer-assisted analysis program.
   1. Label the area 0.5-1.0 disc diameters away from the optic disc margin as zone B, and the area 0.5-2.0 disc diameters away from the optic disc margin as zone C[18] (**Figure 6A**), according to the modified protocol of Atherosclerosis Risk in Communities (ARIC) study[19].
   2. Measure retinal vascular caliber from both zone B and zone C, using a widely-adopted method that is modified from the ARIC study[19,20,21,22,23,24,25,26] (**Figure 6B**).
      1. Measure the lengths of vessel covers in the six largest arterioles and the six largest venules to estimate retinal vessel calibers.
      2. Summarize the retinal arteriolar and venular calibers as central retinal artery equivalent (CRAE) and central retinal vein equivalent (CRVE) respectively[17], using the revised Knudtson–Parr-Hubbard formula[18,19].
   3. Identify all vessels in zone C with a width >40 µm. Calculate the retinal arteriolar and venular tortuosity from the integral of the total squared curvature along the vessel tracings and normalize the value with the total arc length, bowing, and points of inflection[27,28].
   4. Compute the total, arteriolar, and venular fractal dimensions from zone C, using the established "box-counting method"[29,30,31].
      1. Divide the image into a series of equally sized squares.
      2. Count the number of boxes containing a section of the vessel tracings.
      3. Repeat the process using a series of equally sized squares with different sizes.
      4. Plot the logarithm of the number of boxes containing the vessel tracings against the logarithm of the size of the boxes, and calculate the slope of the resulting line; this is the fractal dimension.
   5. Identify vessels with first bifurcation in zone C and calculate the angles (θ) subtended between the first two daughter vessels[32] (**Figure 6C**). Compute the mean value to obtain the average branching angle.
   6. Calculate the branching coefficient from zone C using the formula:
      $(d_1^2 + d_2^2)/d_0^2$, where d_0 is the mean trunk caliber, and d_1 and d_2 are the mean branch calibers (**Figure 6C**).

6. Close the grading window. Click "send" in the pop-up dialog to upload the graded image to the cloud-based server and record the automatically measured retinal vascular parameters.

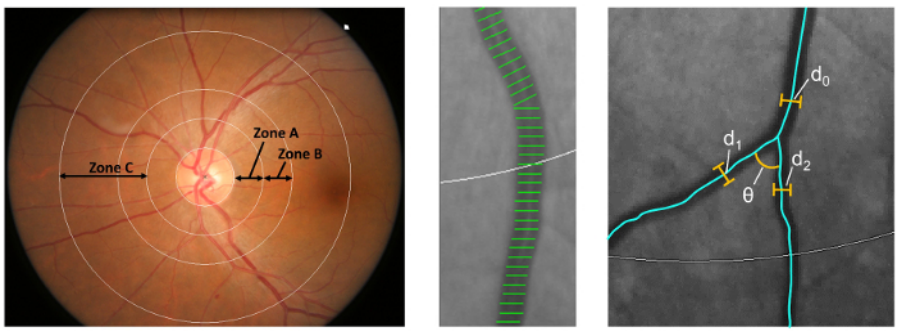

Figure 6: Quantification of retinal vasculature. (**A**) Zone B (defined as 0.5-1.0 disc diameters away from the disc margin) is used to measure vessel calibers of zone B according to the Atherosclerosis Risk in Communities Study. Zone C (defined as 0.5-2.0 disc diameters away from the disc margin) is used to measure vessel calibers of zone C and a spectrum of retinal vascular network parameters (such as tortuosity, fractal dimension, and bifurcation). (**B**) Vessel covers are measurement lines used to estimate the retinal vessel calibers (or diameters). Incorrect vessel covers should be manually excluded from the measurement. (**C**) For all vessels that have their first bifurcation within zone C, the program automatically measures the branching angles (θ) of the first bifurcation. In addition, the branching coefficient is also calculated using the formula: Branching coefficient = $(d_1^2 + d_2^2)/d_0^2$, where d_0 is the trunk caliber, and d^1 and d^2 are the branch calibers. Please click here to view a larger version of this figure.

3. Assess the Thickness of GC-IPL and RNFL

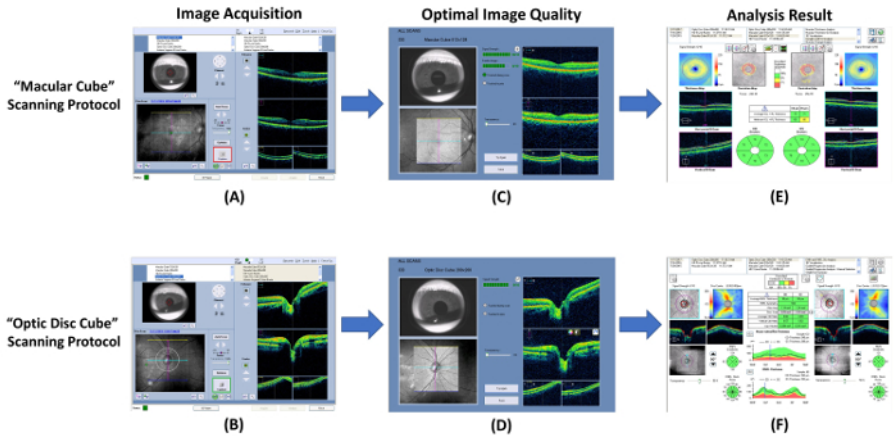

Figure 7: Schematic diagram showing the procedures of measuring RNFL and GC-IPL thickness. Optical coherence tomography (OCT) can be used to measure thicknesses of the ganglion cell-inner plexiform layer (GC-IPL) and the retinal nerve fiber layer (RNFL). (**A, B**) Measure the GC-IPL and RNFL thicknesses using the built-in "macular cube" and "optic disc cube" scanning protocols respectively. (**C, D**) Check the image quality immediately after image acquisition. Discard the image and repeat the scan if the signal strength is smaller than 6, or motion artefacts are detected. (**E, F**) Then, prompt the built-in analysis program to automatically analyze the scan result and generate a report for interpretation. Please click here to view a larger version of this figure.

1. **Perform image acquisition using optical coherence tomography (OCT).**
    1. Open the OCT program and select the "Macular Cube" scanning protocol to start a new macular scan (**Figure 7A**).
    2. Locate the pupil in the iris viewport by adjusting the chinrest. Lower the illumination if the pupil size is too small.
    3. Click the "Auto Focus" button and then the "Optimize" button to improve the image quality.
    4. Instruct the subject to blink a few times immediately before starting the scan.
    5. Click the "Capture" button to start the scan when the border surrounding the button becomes green. Instruct the subject to focus on the visual fixation target during image acquisition to avoid motion artifacts.
    6. Review the scan quality using **Figure 7C** as a standard. Discard the scan result and repeat the scan if the signal strength is smaller than 6 (**Figure 8A**), or motion artefacts are detected (indicated by discontinuity of blood vessels) (**Figure 8B**).
    7. Save the scan result.
    8. Repeat Steps 3.1.1 to 3.1.7 for another eye.
    9. Perform an optic nerve head scan with the "Optic Disc Cube" scanning protocol following steps 3.1.2 to 3.1.9 (**Figures 7B** and **7D**).

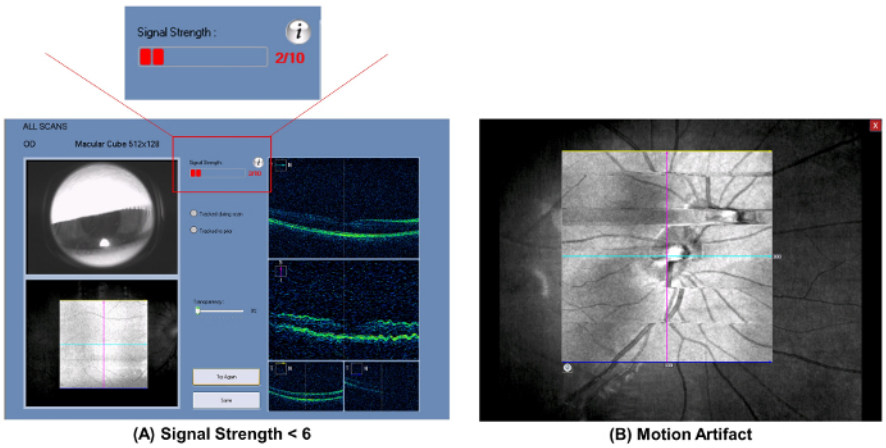

Figure 8: Sub-optimal results of optical coherence tomography. Common sub-optimal results of the optical coherence tomography (OCT) include (**A**) poor signal strength (strength value <6), and (**B**) motion artefacts. The scan quality should be reviewed immediately after image acquisition, and the scan should be repeated if these artefacts are encountered. Please click here to view a larger version of this figure.

2. **Generate an analysis printout of the macular GC-IPL thickness.**
    1. Select the "Macular Cube" scan records of both eyes in the analysis interface.
    2. Click the "Ganglion Cell OU Analysis" to initiate the automatic analysis algorithm to assess the GC-IPL thickness of the scan (**Figure 7E**).
    Note: Step 3.2.2 is automatically completed by the analysis algorithm.

1. Generate a 14.13 mm^2 fovea-centered elliptical annulus that has horizontal inner and outer radiuses of 0.6 mm and 2.4 mm, respectively, and vertical inner and outer radiuses of 0.5 mm and 2.0 mm, respectively.
   Note: The size and shape of the elliptical annulus conform closely to the macular anatomy and thus correspond to the area where the RGCs are thickest in normal eyes[33,34]. The area within the inner ring of the annulus is not measured, as the GC-IPL in this area is very thin.
2. Segment the outer boundary of the RNFL and the outer boundary of the inner plexiform layer (IPL) to locate the GC-IPL (**Figure 9**).
3. Measure the average, minimum, and six sectorial (superotemporal, superior, superonasal, inferonasal, inferior, inferotemporal) thicknesses of macular GC-IPL within the fovea-centered elliptical annulus.
4. Compare the measured GC-IPL thicknesses to the device's internal normative age-matched database and generate a deviation map and a significance map
5. Report the measurement results on an analysis printout.

3. Save the analysis printout in the .pdf format.

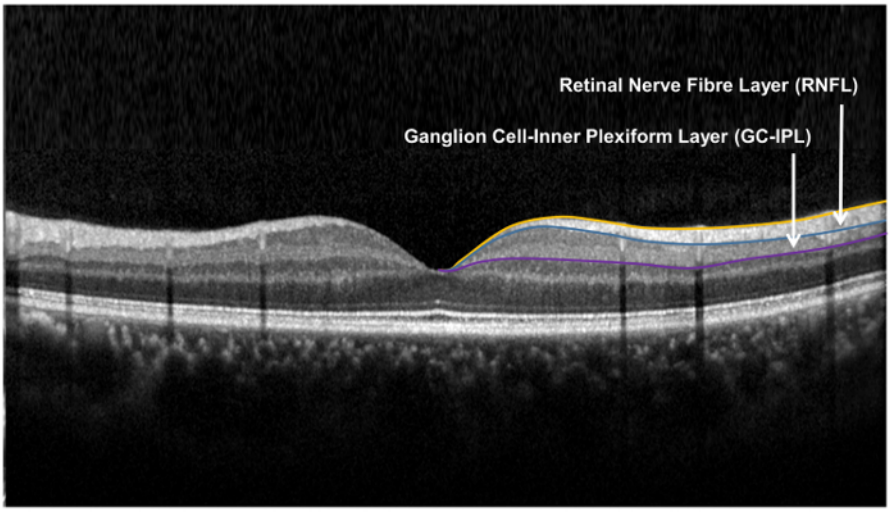

Figure 9: Retinal layers used for the assessment of the retinal neuronal structure. The retinal nerve fibre layer (RNFL) is measured using the optic nerve head (ONH) algorithm, while the ganglion cell-inner plexiform layer is measured using the ganglion cell analysis (GCA) algorithm. The ONH algorithm segments the inner and outer boundary of the RNFL to measure the thickness of RNFL. The GCA algorithm detects the outer boundary of the retinal nerve fiber layer (RNFL) and the inner plexiform layer (IPL) to yield the combined thickness of the ganglion-cell layer (GCL) and the IPL. The thicknesses of GCL and the IPL are measured together, as the boundary between GCL and IPL is anatomically indistinct. However, the combined thickness of GCL and IPL (*i.e.* GC-IPL) is still indicative of the health of RGCs. Please click here to view a larger version of this figure.

3. **Generate the analysis printout of the RNFL thickness (Figure 7F).**
   1. Select the "Optic Disc Cube" scan records of both eyes in the analysis interface.
   2. Click the "ONH and RNFL OU Analysis" to initiate the automatic analysis algorithm to assess the RNFL thickness of the scan.
      Note: Steps 3.3.2.1 to 3.3.2.6 can be automatically completed by the analysis algorithm.
      1. Measure the RNFL thickness at each scan point and generate an RNFL thickness map.
      2. Identify the optic disc by detecting a dark spot near the center of the scan that has a size and shape consistent with the range of an optic disc.
      3. Position a measurement grid of 3.46 mm in diameter around the optic disc on the RNFL thickness map.
      4. Measure and calculate the global, four-quadrants (temporal, superior, nasal and inferior), and twelve-clock-hour parapapillary RNFL thicknesses of the measurement grid.
      5. Compare the measured RNFL thicknesses to the device's internal normative age-matched database and generate a deviation map and a significance map.
      6. Report the measurement results on an analysis printout.

   3. Save the analysis printout in the .pdf format.

Representative Results

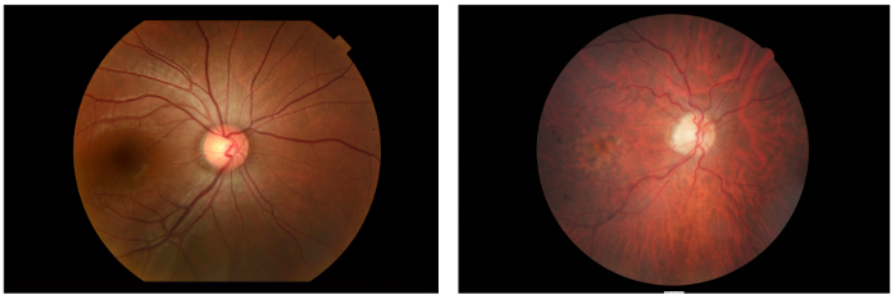

Figure 10: An example to show the differences in retinal vasculature between a normal subject and an AD subject. When compared to the normal subject, fundus photograph of the AD subject showed narrower vessel calibers (CRAE of Zone B, 116.4 µm *vs.* 156.4 µm; CRVE of Zone B, 186.9 µm *vs.* 207.5 µm; CRAE of Zone C, 138.5 µm *vs.* 165.8 µm; CRVE of Zone C, 206.6 µm *vs.* 232.2 µm), smaller retinal vascular fractal dimensions (total fractal dimension, 1.472 *vs.* 1.517; arteriolar fractal dimension, 1.246 *vs.* 1.316; venular fractal dimension, 1.253 *vs.* 1.273) and higher retinal vascular tortuosities (arteriolar tortuosity [104], 0.61 *vs.* 0.48; venular tortuosity [104], 1.41 *vs.* 0.50). These images were captured using a 50-degree fundus camera and were analyzed using the method described in the protocol. Please click here to view a larger version of this figure.

Interpretation of the Retinal Vascular Parameters: With our protocol, retinal vascular parameters can be measured from the fundus photographs. These parameters indicate the status of the retinal vasculature, which may in turn reflect similar changes in the cerebral vasculature. **Figure 10** shows the fundus photographs obtained from an AD subject and a healthy subject. The retinal vascular parameters reported in **Table 1** were measured from these fundus photographs using the method described in this protocol.

	AD	Normal
CRAE of Zone B (µm)	116.4	156.4
CRVE of Zone B (µm)	186.9	207.5
CRAE of Zone C (µm)	138.5	165.8
CRVE of Zone C (µm)	206.6	232.2
Total Fractal Dimension	1.472	1.517
Arteriolar Fractal Dimension	1.246	1.316
Venular Fractal Dimension	1.253	1.273
Arteriolar Tortuosity ($x10^4$)	0.61	0.48
Venular Tortuosity ($x10^4$)	1.41	0.50
Arteriolar Branching Coefficient	2.43	1.49
Arteriolar Branching Angle (deg)	67.17	81.16
Venular Branching Coefficient	1.42	1.62
Venular Branching Angle (deg)	60.11	73.19

Table 1: Differences in Retinal Vascular Parameters between an AD subject and a normal subject. The retinal vascular parameters were measured from the fundus photographs shown in **Figure 10**. When compared to the normal subject, the AD subject showed reductions in vessel calibers (*i.e.* CRAE and CRVE) and fractal dimension, but showed an increase in tortuosity. In addition, the branching angles and branching coefficients of the AD subject also deviated from respective optimal values.

Retinal Vessel Calibers
When compared to the normal subject, the fundus photograph of the AD subject (**Figure 10**) showed decreases in both CRAE and CRVE of Zone C (138.47 µm and 206.61 µm, respectively), when compared to the healthy subject (165.82 µm and 232.22 µm, respectively). The CRAE and CRVE summarize the retinal vessel calibers, which approximate the width of internal lumen in retinal arterioles and venules, respectively. Hence, reductions in CRAE and CRVE indicate generalized narrowing in both retinal arterioles and venules, and suggest microvascular dysfunction[35].

Retinal Vascular Network Parameters
Firstly, the retinal arteriolar and venular tortuosities of the AD subject (0.613×10^{-4} and 1.41×10^{-4}, respectively) were higher than that of the normal subject (0.476×10^{-4} and 0.501×10^{-4}, respectively). The higher vascular tortuosities indicate that the retinal vessels are generally straighter in the AD subject.

Secondly, the AD subject also had reduced retinal fractal dimensions (total fractal dimension, 1.472; arteriolar fractal dimension, 1.246; venular fractal dimension, 1.253) when compared to the healthy subject (total fractal dimension, 1.517; arteriolar fractal dimension, 1.316; venular

fractal dimension, 1.273). Since fractal dimensions represent “global” measures that summarize the branching complexity of the retinal vascular network30, reduced fractal dimensions indicate that the retinal vasculature is less complex in the AD subject.

Thirdly, most retinal bifurcation parameters of the AD subject deviated from the optimal value. Specifically, the arteriolar and venular branching angles of the AD subject (67.17° and 60.109°, respectively) were further away from optimal values, which are approximately 75° [36], when compared with the normal subject (81.16° and 73.19°, respectively). Furthermore, the arteriolar branching coefficient of the AD subject (2.432) also severely deviated from the optimal value, which is approximately 1.26[36]. This represents an increase in total cross-sectional area across the bifurcations[37].

Interpretation of Retinal Neuronal Parameters

With our protocol, one should be able to obtain two analysis printouts showing the average and sectorial thicknesses of RNFL and GC-IPL (illustrated by **Figure 11A** and **11B**, respectively). While the RNFL measurements reflect the health of unmyelinated axons of RGCs, the GC-IPL measurements indicate the health of cell bodies and dendrites of RGCs. Since the size of RGC cell body is 10-20 times the diameter of their axon, GC-IPL thickness has been shown to be more strongly related to cognitive impairment[38].

In both reports, three maps were shown to aid the interpretation, namely (a) thickness maps, (b) deviation maps, and (c) significance maps. In the thickness maps, warmer colors represent higher thickness values and cooler colors represent lower thickness values; in other words, the denser the orange/yellow ring, the thicker the retinal layer concerned. The software also compares the measured thicknesses to the device’s internal normative age-matched database, and generates deviation maps and significance maps. In the deviation maps, a super-pixel is shown in red or yellow if the thickness value falls outside the 99% or within 95–99% centile range, respectively. In the significance maps, the retinal layer concerned is divided into different sectors, as the retina is unlikely to be homogeneously affected by dementia. The thickness value of each sector is reported and each sector is also color-coded to match the comparison result, with values within the normal range in green (p = 5–95%), borderline values in yellow (1%<p<5%), and values outside the normal range in red (p <1%).

The analysis printouts of RNFL and GC-IPL in an AD subject are shown in **Figure 11A** and **Figure 11B** respectively. The fading of warm colors and the appearance of light blue areas in the thickness maps of both reports indicates thinning of GC-IPL and RNFL in the AD subject. While thinning of GC-IPL suggests RGC loss, thinning of RNFL suggests loss of RGC axons. In addition, several sectors of the significance maps are labelled in red or yellow, suggesting that the RNFL and GC-IPL thicknesses of the corresponding areas are reduced in the AD subject. The exact areas of thinning can also be visualized by the red or yellow super-pixels in the deviation maps.

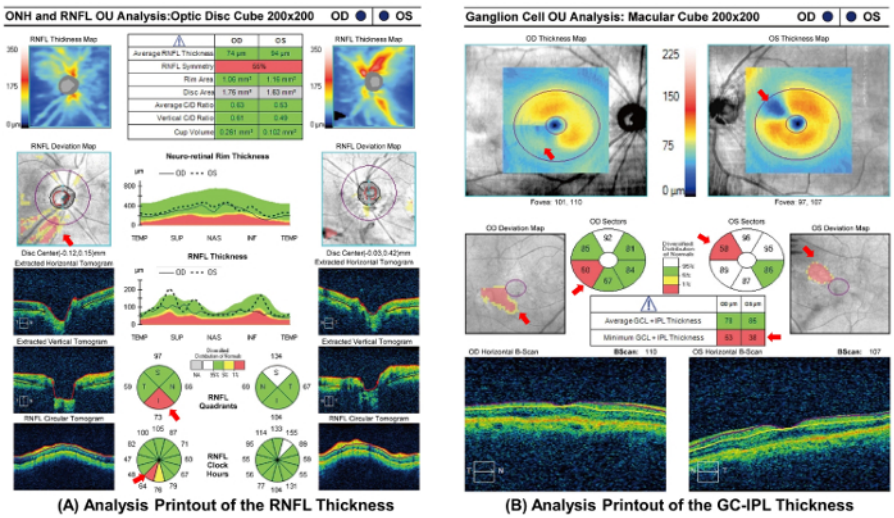

Figure 11: Analysis printout of retinal neuronal structure from an AD subject. Thinning of RNFL and GC-IPL in the AD subject is indicated by the presence of more light blue areas in the thickness maps. The magnitude of thinning is considered abnormal after compared to the normative age-matched population; the red sectors indicate the thickness value of the corresponding areas fell outside the normal range (p <1%), while the yellow sector indicates borderline value in the corresponding area (1%<p< 5%). The exact areas of RNFL and GC-IPL thinning can also be visualized by the deviation maps, in which the red and yellow super-pixels (red arrows) indicate the thickness values of the corresponding spots fell outside the 99% or within 95–99% percentile range, respectively. All together, these maps suggest that both RNFL and GC-IPL thicknesses were abnormally reduced in the AD subject. Please click here to view a larger version of this figure.

Unanalyzable or Ungradable Retinal Images: Fundus photographs or OCT scans may be unanalyzable owing to several reasons. Regarding OCT scans, GC-IPL or RNFL segmentation failure may occur due to retinal pathologies, such as age-related macular degeneration, diabetic retinopathy, and epiretinal membrane. **Figure 12A** demonstrates an example of segmentation failure due to diabetic macular edema. It has also been shown that OCT scan quality and thickness measurements can be affected by dry eyes[39], cataracts[40,41,42,43], floaters and other vitreous opacities[44,45]. Regarding fundus photographs, the measurement of retinal vascular parameters may also be hindered by media opacity (such as a cataract), which affects the visibility of the retinal vasculature (**Figure 12B**).

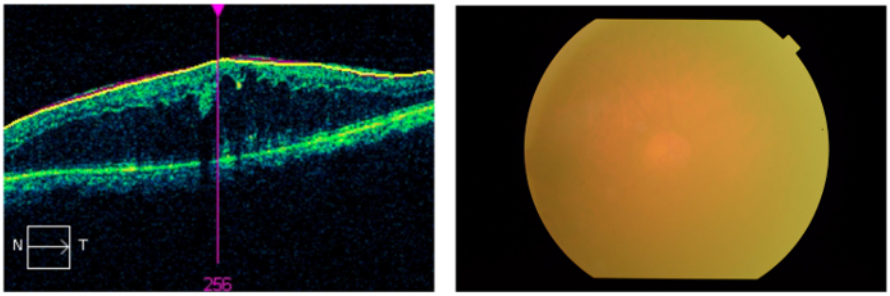

Figure 12: Unanalyzable retinal images. While most suboptimal results could be avoided using the methods described, several types of retinal images are unanalyzable and should be discarded. (**A**) Segmentation failure may occur in some OCT scans due to retinal pathologies, including age-related macular degeneration, diabetic retinopathy, and epiretinal membrane. This figure demonstrates a segmentation failure due to diabetic macular edema. (**B**) The visibility of the retinal vasculature can be reduced by media opacity, such as opacity due to a cataract. This figure demonstrates that severe media opacity can obscure the retinal vasculature and render the image unanalyzable. Please click here to view a larger version of this figure.

Parameter	Measured Zone	Interpretation and Reported Association with AD
Retinal Vessel Caliber		
Central Retinal Arteriolar Equivalent (CRAE)	Zone B & C	♦ Changes in Central retinal arteriolar equivalent (CRAE) and central retinal venular equivalent (CRVE) indicate generalized retinal vessel narrowing or widening, and may suggest subtle microvascular dysfunction[35]. ♦ It has been reported that increased CRVE is associated with incident dementia[46], vascular dementia[46], and decreased CRVE and CRAE are associated with Alzheimer's Disease[47,48].
Central Retinal Venular Equivalent (CRVE)	Zone B & C	
Retinal Vascular Network Parameters		
Fractal Dimensions (dF)	Zone C	♦ Fractal dimension represents a "macro" measure that summarizes the branching complexity of the retinal vascular network[30]; a larger value indicates a more complex branching pattern. ♦ It has been suggested that reduced retinal fractal dimension was associated with dementia[47,48,59] and cognitive function[60].
Tortuosity (TORT)	Zone C	♦ Tortuosity reflects the general straightness of the retinal vessels, with a smaller tortuosity value indicates straighter retinal vessels. ♦ It has been suggested that increased venular tortuosity and arteriolar tortuosity are associated with AD[62].
Branching Angle (BA)	Zone C	♦ The optimal value of BA is approximately 75°[36] ♦ Alteration in branching angle may indicate changes in blood flow[63,64], endothelial dysfunction[65,66] and attenuation in oxygen saturation[67].
Branching Coefficient (BC)	Zone C	♦ The optimal value of BC is approximately 1.26[36]. ♦ Deviation from the optimal value may increase energy cost, reducing the efficiency of circulation and metabolic transport[37].

Table 2: Interpretations of major retinal vascular parameters. Vessel calibers and retinal vascular network parameters are two main categories of parameters reported by the computer-assisted analysis program. CRAE and CRVE document generalized retinal vessel narrowing or widening, reflecting subtle retinal microvascular dysfunction. Retinal vascular network parameters capture the "optimality" and "efficiency" of blood distribution in the retinal network, which in turn reflect the integrity of the cerebral microcirculation.

Discussion

This protocol describes the procedures of quantifying neuronal and vascular changes in the retina *in vivo*. As the retina shares similar embryological origins, anatomical features and physiological properties with the brain, these retinal changes may reflect similar changes of vasculature and neuronal structure in the brain.

As shown in **Figure 10** and **Table 1**, the AD subject showed decreased vessel calibers when compared to the healthy subject. It has been reported that decreased CRVE and CRAE are associated with Alzheimer's Disease[46,47], although this is not consistently observed[48].

Furthermore, the AD subject also showed decreased fractal dimensions, increased vascular tortuosities, and suboptimal branching coefficients and branching angles when compared to the healthy subject. These changes indicate alterations in global geometrical patterns of the retinal vascular network[49,50,51,52,53,54,55,56]. Since the branching pattern of the vascular network, according to Murray's principle, is structurally developed to minimize the energy required to maintain blood flow[57], these parameters also capture the degree of "optimality" and "efficiency" of blood distribution in the retinal vascular network, which may in turn reflect the integrity of the cerebral microcirculation[58]. It has been reported that reduced retinal fractal dimension is associated with dementia[47,48,59] and cognitive function60,and is potentially related to microvascular damages leading to retinal hypoxia[61]. Increased venular and arteriolar tortuosities are also shown to be associated with AD[62]. Regarding the retinal bifurcation parameters, sub-optimality of the branching angles indicates that the retinal vascular network in the AD subject has decreased efficiency of tissue perfusion and increased energy loss[37]. Alteration in branching angle may also indicate changes in blood flow[63,64],

endothelial dysfunction[65,66], and attenuation of oxygen saturation[67]. In addition, deviation from the optimal value of the branching coefficient may also increase energy cost, reducing the efficiency of circulation and metabolic transport[37]. Taken together, changes in vascular network parameters (i.e. *fractal dimension, tortuosity, branching angle and branching coefficient*) suggest the microvascular involvement in AD pathology. The reported associations of major retinal vascular parameters with AD are summarized in **Table 2** and have also been reviewed in details previously[8,58,68,69].

As illustrated by **Figure 11**, the AD subject also showed decreased thicknesses of RNFL and GC-IPL. Although the thicknesses of GCL and IPL can only be reported together owing to their ambiguous anatomical boundary, the combined thickness (*i.e.* GC-IPL) is indicative of the health of RGCs[38]. It is increasingly evident that thinning of GC-IPL[38] and RNFL[70,71,72,73,74,75,76,77,78] is associated with AD. Recently, a large-scale population study also reported that thinner RNFL is associated with poorer cognitive function, such as poorer prospective memory, and poorer performance of numeric and verbal reasoning[79]. In addition, thinning of RNFL is also reported in non-AD dementias[80,81,82].

Critical Steps of Retinal Imaging

Several steps in the protocol must be performed correctly in order to obtain an accurate result. Regarding the procedure of image acquisition, it is important to master the imaging procedure of OCT and fundus photography, since a prolonged imaging time may induce eye fatigue and thus increase the likelihood of motion artefacts. In addition, contrast and saturation of the images should be standardized during image acquisition to avoid coarse adjustment in the later steps of image processing. The contrast and the saturation can be varied with different study cohorts and camera types.

Regarding the measurement of retinal vascular parameters, it is important to calculate the ICF for every camera used in the study to adjust for the magnification effect and the difference in image resolution. Adjustment by ICF is important for the accurate measurement of dimensional parameters, including retinal vessel calibers. In addition, when grading the fundus photographs with a computer-assisted analysis program, graders should be masked to the participant's characteristics as the grading process involves a certain amount of manual adjustment. Also, the graders should receive proper training and their reliability of measurement should be evaluated first, before grading the images.

It is also important to report retinal vessel caliber in both zone B and zone C. It is believed that the vessel caliber of zone C is more sensitive and more precise with smaller standard error[17], possibly due to inclusion of more peripheral small vessels in the retina, which are anatomically and physiologically more similar to the small vessels in the brain. However, the caliber of zone B should also be reported as the caliber measurement within zone B has been widely used in numerous epidemiological studies.

It should be noted that the equipment and the computer-assisted analysis program used in this protocol are for illustration purposes only and similar results can be obtained using other retinal imaging techniques. However, in most cases the numerical parameters reported by different measurement systems should not be interpreted interchangeably[83]. Yip et al. have developed an algorithm for conversion between three commonly used software measuring retinal vessel calibers, which may be useful to compare results from different studies[83].

Significance of Retinal Imaging

Magnetic Resonance Imaging (MRI) and Positron Emission Tomography (PET) imaging are two widely used in vivo imaging methods to study dementia. However, the application of MRI is limited by its spatial resolution to detect subtle degenerative changes of less than 500 µm. The use of PET imaging is also limited by its high cost and the availability of PET facilities. In addition, although cerebral small vessel disease has been linked to dementia[84,85,86,87,88,89,90], current neuroimaging technologies do not allow direct assessment of the cerebral small-vessel changes, such as cerebral arteriolar narrowing, changes in vascular tortuosity, and capillary micro-aneurysm. Hence, a complementary approach to study dementia is desired. Retinal imaging demonstrates several features that make it different from other neuroimaging techniques and allow it to provide new insights to dementia research.

Firstly, the retina is highly accessible for non-invasive imaging when compared with other parts of the CNS. As the pupil allows bidirectional passage for the illuminating and imaging light rays, the retinal vascualture can be imaged directly and rapidly using a fundus camera, which is a classic retinal imaging technique based on the principle of monocular indirect ophthalmoscopy. Fundus photography has demonstrated high sensitivity, specificity, and inter-examination and intra-examination agreement[91]. Furthermore, *in vivo* cross-sectional images of retinal neuronal structure can also be captured by OCT based on the principle of low-coherence interferometry[92,93,94,95,96]. As a result, retinal imaging allows longitudinal and non-invasive imaging with relatively low costs to observe the effect of dementia on CNS.

Secondly, the retinal neuronal structure is organized as distinguishable layers and each layer represents a specific element of the neuronal architecture. For instance, the GC-IPL represents the cell bodies and dendrites of RGCs, while the RNFL represents the axons of RGCs. Notably, accurate demarcation of retinal neuronal layers, such as GC-IPL and RNFL, can now be achieved with advanced segmentation algorithms[33,97], and any dementia pathology that manifests as a distortion of neuronal architecture can be easily detected.

Thirdly, objective, semi-automated, and standardized assessment of retinal images is now possible using computer-assisted analysis programs. As illustrated by this protocol, the computer-assisted analysis programs can automatically trace the retinal vasculature captured by the fundus photography and, based on the tracing results, measure a spectrum of retinal vascular parameters, such as vessel calibers, tortuosities, fractal dimensions, and branching angles. During the tracing process, the graders are only required to verify the accuracy of vessel tracings and, if necessary, adjust incorrect vessel tracings manually. Previous studies have reported that intragrader and intergrader reliability were moderate to high[49]. Similarly, the OCT built-in analysis algorithms can also automatically measure parameters of RNFL and GC-IPL thicknesses, and compare the results with the normative age-matched databases[98]. The semi-automatic nature of retinal imaging helps to improve measurement efficiency and consistency by reducing the amount of work required from each grader. Graders can also rapidly master the skills of measuring and interpreting retinal parameters, without learning too much advanced ophthalmological or neurological knowledge. Hence, retinal imaging can be easily applied in a populational setting.

Lastly, retinal imaging technologies can now image the retina at resolution of several microns, which is at least an order of magnitude than that can be achieved with conventional neuroimaging techniques. For instance, the spectral domain-OCT can now image the retina in three-dimensional volume with a high axial resolution (*e.g.* several microns) and a high degree of reproducibility[99,100,101,102,103,104,105]. This allows direct

visualization and quantification of subtle changes in the retina including the RGC axons, the ocular extension of the CNS. The associations between dementia and microvascular changes can also be directly assessed by measuring retinal vascular parameters.

Taken together, retinal imaging can collect unique information on the cerebral vasculature and neuronal structure that is distinct from current brain imaging techniques, suggesting that retinal imaging may provide a complementary approach to study the pathology of dementia[9,35,58,68,106,107,108].

Limitations of the Method

Retinal imaging is an increasingly popular method to visualize and quantify microvasculature and neuronal structure in the retina[8,109]. However, readers of this protocol should be aware of its potential limitations in order to interpret the results critically.

First, the quality of fundus photographs and OCT images can be affected by a range of ocular factors. For instance, variations in refractive error and axial length may affect the magnification and therefore the apparent dimensions of retinal vascular caliber [110]. Differences in retinal pigmentation, presence of media opacities, photographic technique, camera type (*e.g.*, mydriatic, non-mydriatic, hand-held), and image quality (*e.g.*, brightness, focus, and contrast) may also introduce additional sources of variation and affect measurements[111,112,113,114,115,116]. In addition, motion artefacts may be common in old-aged subjects if the image acquisition is prolonged.

Second, the retinal vascular and neuronal architecture can be affected by many systemic and local pathological processes, and thus some retinal manifestations are not specific to a particular disease. For instance, retinal arteriolar narrowing has been correlated to systemic peripheral vasoconstriction and hypertension, while retinal venular widening has been correlated to endothelial dysfunction, inflammation, microvascular hypoxia[117], and diseases such as cardiovascular disease[118] and diabetic retinopathy[119]. RNFL thinning is also observed in other neurodegenerative diseases, including glaucoma, Parkinson's Disease, and multiple sclerosis[10]. It is also noteworthy that age-related reduction in RGCs and their axons can also occur without dementia[99,120].

Third, the associations between retinal changes and dementia remain inconclusive. For instance, the associations of smaller vessel calibers with AD were not replicated by Williams *et al.*[59], and the association of narrower arteriolar caliber with AD found by the Singapore Epidemiology of Eye Disease program study was also lost after adjusting for confounding cardiovascular factors[48]. Furthermore, increased venular and arteriolar tortuosities in AD are also not consistently observed[47,59]. It is also noted that the association of arteriolar fractal dimension with dementia was lost in a fully adjusted model[59].

Fourth, the computer-assisted analysis programs at this stage are only semi-automated and require manual adjustments by trained graders[49,121]. Manual inputs, even following a standardized protocol, may introduce additional variability in the retinal measurements.

Future applications of the method

Given the accessibility of the retina and its similarities to other parts of CNS, the retina is an excellent "window" for studying the effect of dementia on cerebral microvasculature and neuronal structure. Since dementia is now thought to involve vascular processes[84,85,86,87,88,89,90,122], imaging and quantifying retinal microvasculature using this protocol may also provide new insights into the microvascular etiology (versus macrovascular etiology) of dementia[10,35,58,106,108,123] and facilitate our understanding on different dementia subtypes.

In addition, retinal imaging might potentially be used in clinical settings to facilitate the preclinical diagnosis or risk assessment of dementia, to confirm clinically diagnosed AD, and to monitor the disease progression or response to therapy. The application of retinal imaging in population screening is particularly intriguing as neuronal and microvascular changes, which might be reflected by similar retinal changes, occur much earlier than the appearance of cortical atrophy and cognitive decline[124,125]. Consistently, studies have shown that RNFL and GC-IPL thicknesses were reduced in patients with mild cognitive impairment (MCI) and AD when compared with health controls, but the differences in RNFL and GC-IPL thicknesses between patients with MCI and those with AD were not statistically significant[8], suggesting that thinning of RNFL and GC-IPL is an early event in AD pathology. However, the strength of associations between retinal imaging measures and dementia is only modest and several retinal correlates of AD have not been consistently observed[8,47,48,59,109]. This protocol can potentially be adopted by more prospective clinical studies with large cohorts to evaluate the clinical utility of retinal imaging in the pre-clinical diagnosis of AD.

Recent advances in retinal imaging techniques, such as the ultra-wide field retinal imaging and the OCT-angiography, may allow us to obtain more information from the retina. The ultra-wide field retinal imaging technology, based on the principle of confocal laser scanning microscopy combined with a concave elliptical mirror, can capture up to 200° of the retina in a single image without pupil dilation[126,127]. This allows more extensive assessment of peripheral retinal lesions, which may provide more information on the overall retinal vasculature[17]. It has been reported that the ultra-wide field retinal imaging can achieve satisfactory performance in both vessel segmentation and width estimation[128]. In addition, the invention of OCT-angiography also allows non-dye-based mapping of the retinal capillary network, which might provide more information on microvascular changes related to dementia. In view of image analysis methods, more research is required to explore other state-of-the-art image processing and quantitative methods, such as tree topology estimation[129], to analyze the images captured by these novel imaging modalities.

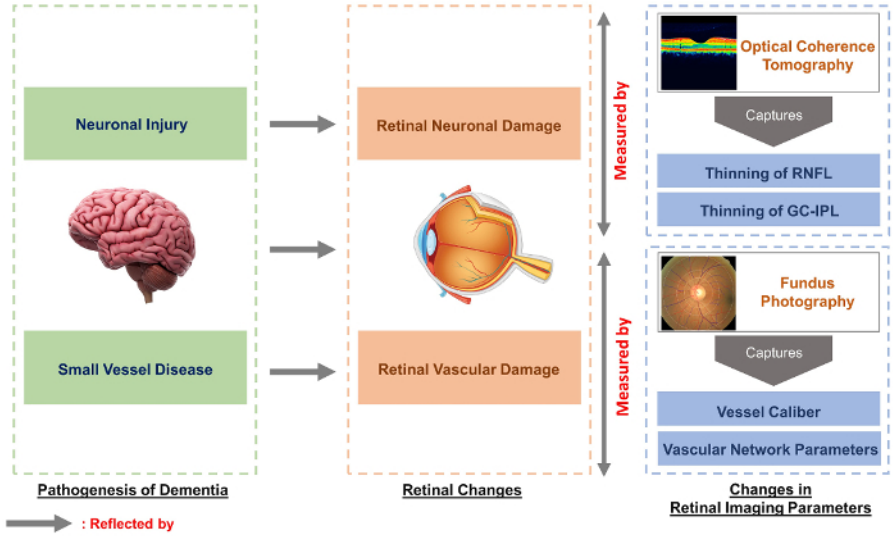

Figure 13: Retinal imaging is a potentially valuable tool to study vascular and neuronal changes associated with dementia. It has been proposed that dementia is associated with neuronal injury and small vessel disease in the brain. As the retina, being an extension of the central nervous system, shares prominent similarities with the brain, these pathological changes may be reflected in the retina as retinal neuronal and vascular damages. Using this protocol, the retinal neuronal changes can be quantified as changes in RNFL and GC-IPL thicknesses using optical coherence tomography (OCT), while the retinal vascular changes can be quantified as changes in vessel calibers and vascular network parameters using fundus photography and a computer-assisted analysis program. Studying the associations between the retinal changes and dementia may provide new insights into the pathology of dementia and, potentially, aid in diagnosis and risk assessment. Please click here to view a larger version of this figure.

This protocol describes a non-invasive, quantitative and semi-automated method to study dementia using retinal imaging techniques (**Figure 13**). Considering the accessibility of retina and its robust associations with the brain, imaging the retina may provide new insights into dementia and, potentially, aid in the diagnosis and risk assessment of dementia. However, the associations reported at this stage remain controversial and further studies are required to assess the potential utility of retinal imaging. It should also be noted that a thorough clinical evaluation remains essential in the assessment of dementia.

Disclosures

Regarding potential financial ties, the author Tien Y. Wong is a co-inventor of the Singapore I Vessel Assessment (SIVA) program used in this article.

Acknowledgements

We would like to express our appreciation to the School of Computing, National University of Singapore for technical support and the Health and Medical Research Fund (04153506), Hong Kong for funding support.

References

1. Alzheimer's Disease International. The prevalence of dementia worldwide. *Alzheimer's Dis. Int.* (December), 1-2 (2008).
2. Wimo, A., Winblad, B., &Jönsson, L. The worldwide societal costs of dementia: Estimates for 2009. *Alzheimer's Dement.* **6** (2), 98-103 (2010).
3. Comas-Herrera, A., Northey, S., Wittenberg, R., Knapp, M., Bhattacharyya, S., & Burns, A. Future costs of dementia-related long-term care: exploring future scenarios. *Int. Psychogeriatr.* **23** (1), 20-30 (2011).
4. Alzheimer's Association. 2014 Alzheimer's disease facts and figures. *Alzheimer's Dement.* **10** (2), e47-e92 (2014).
5. Prince, M., Bryce, R., Albanese, E., Wimo, A., Ribeiro, W., & Ferri, C. P. The global prevalence of dementia: a systematic review and metaanalysis. *Alzheimers. Dement.* **9** (1), 63-75.e2 (2013).
6. Alzheimer's Association. Alzheimer's disease facts and figures. *Alzheimer's Dement.* **12** (4), 459-509 (2016).
7. Asih, P. R., Chatterjee, P., Verdile, G., Gupta, V. B., Trengove, R. D., & Martins, R. N. Clearing the amyloid in Alzheimer's: progress towards earlier diagnosis and effective treatments - an update for clinicians. *Neurodegener. Dis. Manag.* **4** (5), 363-378 (2014).
8. Cheung, C. Y., Ikram, M. K., Chen, C., & Wong, T. Y. Imaging retina to study dementia and stroke. *Prog. Retin. Eye Res.* (2017).
9. Patton, N., Aslam, T., Macgillivray, T., Pattie, A., Deary, I. J., & Dhillon, B. Retinal vascular image analysis as a potential screening tool for cerebrovascular disease: a rationale based on homology between cerebral and retinal microvasculatures. *J. Anat.* **206** (4), 319-48 (2005).
10. London, A., Benhar, I., & Schwartz, M. The retina as a window to the brain-from eye research to CNS disorders. *Nat. Rev. Neurol.* **9** (1), 44-53 (2013).
11. Crowe, M. J., Bresnahan, J. C., Shuman, S. L., Masters, J. N., & Beattie, M. S. Apoptosis and delayed degeneration after spinal cord injury in rats and monkeys. *Nat Med.* **3** (1), 73-76 (1997).

12. Levkovitch-Verbin, H., Quigley, H. A., Kerrigan-Baumrind, L. A., D'Anna, S. A., Kerrigan, D., & Pease, M. E. Optic nerve transection in monkeys may result in secondary degeneration of retinal ganglion cells. *Investig. Ophthalmol. Vis. Sci.* **42** (5), 975-982 (2001).
13. Levkovitch-Verbin, H., Quigley, H. A., Martin, K. R., Zack, D. J., Pease, M. E., & Valenta, D. F. A model to study differences between primary and secondary degeneration of retinal ganglion cells in rats by partial optic nerve transection. *Invest Ophthalmol Vis Sci.* **44** (8), 3388-3393. (2003).
14. Yoles, E., & Schwartz, M. Degeneration of spared axons following partial white matter lesion: implications for optic nerve neuropathies. *Exp Neurol.* **153** (1), 1-7 (1998).
15. Sadun, A. A., Borchert, M., DeVita, E., Hinton, D. R., & Bassi, C. J. Assessment of Visual Impairment in Patients With Alzheimer's Disease. *Am. J. Ophthalmol.* **104** (2), 113-120 (1987).
16. Schlotterer, G., Moscovitch, M., & Crapper-Mclachlan, D. Visual processing deficits as assessed by spatial frequency contrast sensitivity and backward masking in normal ageing and alzheimer's disease. *Brain.* **107** (1), 309-324 (1984).
17. Cheung, C. Y. L. *et al.* A new method to measure peripheral retinal vascular caliber over an extended area. *Microcirculation.* **17** (7), 495-503 (2010).
18. Knudtson, M. D., Lee, K. E., Hubbard, L. D., Wong, T. Y., Klein, R., & Klein, B. E. K. Revised formulas for summarizing retinal vessel diameters. *Curr. Eye Res.* **27** (3), 143-149 (2003).
19. Hubbard, L. D. *et al.* Methods for evaluation of retinal microvascular abnormalities associated with hypertension/sclerosis in the Atherosclerosis Risk in Communities Study. *Ophthalmology.* **106** (12), 2269-2280 (1999).
20. Patton, N. *et al.* The association between retinal vascular network geometry and cognitive ability in an elderly population. *Investig. Ophthalmol. Vis. Sci.* **48** (5), 1995-2000 (2007).
21. VanHecke, M.V *et al.* Are retinal microvascular abnormalities associated with large artery endothelial dysfunction and intima-media thickness? The Hoorn Study. *Clin. Sci. London Engl. 1979.* **110** (5), 597-604 (2006).
22. Tien, Y. W. *et al.* Retinal vascular caliber, cardiovascular risk factors, and inflammation: The Multi-Ethnic Study of Atherosclerosis (MESA). *Investig. Ophthalmol. Vis. Sci.* **47** (6), 2341-2350 (2006).
23. Leung, H. *et al.* Relationships between age, blood pressure, and retinal vessel diameters in an older population. *Investig. Ophthalmol. Vis. Sci.* **44** (7), 2900-2904 (2003).
24. Wong, T. Y. *et al.* The prevalence and risk factors of retinal microvascular abnormalities in older persons: The cardiovascular health study. *Ophthalmology.* **110** (4), 658-666 (2003).
25. Ikram, M. K. *et al.* Retinal vessel diameters and risk of stroke: The Rotterdam Study. *Neurology.* **66** (9), 1339-1343 (2006).
26. Wong, T. Y., Knudtson, M. D., Klein, R., Klein, B. E. K., Meuer, S. M., & Hubbard, L. D. Computer-assisted measurement of retinal vessel diameters in the Beaver Dam Eye Study: Methodology, correlation between eyes, and effect of refractive errors. *Ophthalmology.* **111** (6), 1183-1190 (2004).
27. Sasongko, M. B. *et al.* Alterations in retinal microvascular geometry in young type 1 diabetes. *Diabetes Care.* **33** (6), 1331-1336 (2010).
28. Cheung, C. Y.-L. *et al.* Retinal vascular tortuosity, blood pressure, and cardiovascular risk factors. *Ophthalmology.* **118** (5), 812-8 (2011).
29. Mainster, M. a The fractal properties of retinal vessels: embryological and clinical implications. *Eye.* **4 (Pt 1)** (1), 235-241 (1990).
30. Liew, G. *et al.* The Retinal Vasculature as a Fractal: Methodology, Reliability, and Relationship to Blood Pressure. *Ophthalmology.* **115** (11) (2008).
31. Stosic, T., & Stosic, B. D. Multifractal analysis of human retinal vessels. *IEEE Trans. Med. Imaging.* **25** (8), 1101-1107 (2006).
32. Zamir, M., Medeiros, J. a, Cunningham, T. K., & M. Zamir, J. A. Medeiros, T. K. C. Arterial bifurcations in the human retina. *J. Gen. Physiol.* **74** (4), 537-48 (1979).
33. Mwanza, J. C., Oakley, J. D., Budenz, D. L., Chang, R. T., Knight, O. J., & Feuer, W. J. Macular ganglion cell-inner plexiform layer: Automated detection and thickness reproducibility with spectral domain-optical coherence tomography in glaucoma. *Investig. Ophthalmol. Vis. Sci.* **52** (11), 8323-8329 (2011).
34. Bendschneider, D. *et al.* Retinal nerve fiber layer thickness in normals measured by spectral domain OCT. *J. Glaucoma.* **19** (7), 475-482 (2010).
35. Cheung, C. Y., Ong, Y.-T., Ikram, M. K., Chen, C., & Wong, T. Y. Retinal Microvasculature in Alzheimer's Disease. *J. Alzheimer's Dis.* **42** (s4), S339-S352 (2014).
36. Murray, C. D. THE PHYSIOLOGICAL PRINCIPLE OF MINIMUM WORK APPLIED TO THE ANGLE OF BRANCHING OF ARTERIES. *J. Gen. Physiol.* (4), 835-841 (1926).
37. Ding, J. *et al.* Early retinal arteriolar changes and peripheral neuropathy in diabetes. *Diabetes Care.* **35** (5), 1098-1104 (2012).
38. Yim, C. *et al.* Retinal Ganglion Cell Analysis Using High-Definition Optical Coherence Tomography in Patients with Mild Cognitive Impairment and Alzheimer's Disease. *J. Alzheimer's Dis. Retin. Ganglion Cell Anal. MCI AD.* **45** (1), 45-56 (2015).
39. Stein, D. M., Wollstein, G., Ishikawa, H., Hertzmark, E., Noecker, R. J., & Schuman, J. S. Effect of Corneal Drying on Optical Coherence Tomography. *Ophthalmology.* **113** (6), 985-991 (2006).
40. Mwanza, J. C. *et al.* Effect of Cataract and its Removal on Signal Strength and Peripapillary Retinal Nerve Fiber Layer Optical Coherence Tomography Measurements. *J. Glaucoma.* **20** (1), 37-43 (2011).
41. Garcia-Martin, E. *et al.* Influence of cataract surgery on optical coherence tomography and neurophysiology measurements in patients with retinitis pigmentosa. *Am. J. Ophthalmol.* **156** (2) (2013).
42. Kok, P. H. B. *et al.* The relationship between the optical density of cataract and its influence on retinal nerve fibre layer thickness measured with spectral domain optical coherence tomography. *Acta Ophthalmol.* (2012).
43. Kim, N. R. *et al.* Influence of cataract on time domain and spectral domain optical coherence tomography retinal nerve fiber layer measurements. *J. Glaucoma.* **21** (2), 116-22 (2012).
44. Hwang, Y. H., & Kim, Y. Y. Effect of Peripapillary Vitreous Opacity on Retinal Nerve Fiber Layer Thickness Measurement Using Optical Coherence Tomography. *Arch. Ophthalmol.* **130** (6), 789-792 (2012).
45. Schwartz, S. G., Flynn, H. W., & Fisher, Y. L. "Floater scotoma" demonstrated on spectral-domain optical coherence tomography and caused by vitreous opacification. *Ophthalmic Surg. Lasers Imaging Retina.* **44** (4), 415-8 (2013).
46. Frost, S. *et al.* Retinal vascular biomarkers for early detection and monitoring of Alzheimer's disease. *Transl. Psychiatry.* **3** (2), e233 (2013).
47. Cheung, C. Y. *et al.* Microvascular network alterations in the retina of patients with Alzheimer's disease. *Alzheimer's Dement.* **10** (2), 135-142 (2014).
48. DeJong, F. J. *et al.* Retinal vascular caliber and risk of dementia: The Rotterdam Study. *Neurology.* **76** (9), 816-821 (2011).

49. Cheung, C. Y. *et al.* Quantitative and qualitative retinal microvascular characteristics and blood pressure. *J. Hypertens.* **29** (7), 1380-1391 (2011).
50. Cheung, C. Y. *et al.* Retinal vascular fractal dimension and its relationship with cardiovascular and ocular risk factors. *Am. J. Ophthalmol.* **154** (4), 663-674 (2012).
51. Cheung, C. Y.-L. *et al.* Retinal vascular tortuosity, blood pressure, and cardiovascular risk factors. *Ophthalmology.* **118** (5), 812-8 (2011).
52. Grinton, M. E. *et al.* The association between retinal vessel morphology and retinal nerve fiber layer thickness in an elderly population. *Ophthalmic Surg. Lasers Imaging.* **43** (6 Suppl), S61-6 (2012).
53. Hughes, A. D. *et al.* Quantification of topological changes in retinal vascular architecture in essential and malignant hypertension. *J. Hypertens.* **24** (5), 889-94 (2006).
54. Hughes, A. D. *et al.* Determinants of retinal microvascular architecture in normal subjects. *Microcirculation.* **16** (2), 159-66 (2009).
55. Lau, Q. P., Lee, M. L., Hsu, W., & Wong, T. Y. The Singapore Eye Vessel Assessment System. *Image Anal. Model. Ophthalmol.* , 143-160 (2014).
56. Thomas, G. N. *et al.* Measurement of Macular Fractal Dimension Using a Computer-Assisted Program. *Investig. Opthalmology Vis. Sci.* **55** (4), 2237 (2014).
57. Murray, C. D. The physiological principle of minimal work. I. The vascular system and the cost of blood volume. *Proc. Natl. Acad. Sci.* **12**, 207-214 (1926).
58. Cheung, C., Chen, C., & Wong, T. Ocular Fundus Photography as a Tool to Study Stroke and Dementia. *Semin. Neurol.* **35** (5), 481-490 (2015).
59. Williams, M. A. *et al.* Retinal microvascular network attenuation in Alzheimer's disease. *Alzheimer's Dement. Diagnosis, Assess. Dis. Monit.* **1** (2), 229-235 (2015).
60. Cheung, C. Y. *et al.* Retinal Vascular Fractal Dimension Is Associated with Cognitive Dysfunction. *J. Stroke Cerebrovasc. Dis.* **23** (1), 43-50 (2014).
61. Hammes, H.-P. *et al.* Diabetic retinopathy: targeting vasoregression. *Diabetes.* **60** (1), 9-16 (2011).
62. Cheung, C. Y. *et al.* Microvascular network alterations in the retina of patients with Alzheimer's disease. *Alzheimer's Dement.* **10** (2), 135-142 (2014).
63. Frame, M. D., & Sarelius, I. H. Arteriolar bifurcation angles vary with position and when flow is changed. *Microvasc Res.* **46** (2), 190-205 (1993).
64. Djonov, V., Baum, O., & Burri, P. H. Vascular remodeling by intussusceptive angiogenesis. *Cell Tissue Res.* **314** (1), 107-117 (2003).
65. Griffith, T. M., & Edwards, D. H. Basal EDRF activity helps to keep the geometrical configuration of arterial bifurcations close to the Murray optimum. *J. Theor. Biol.* **146** (4), 545-73 (1990).
66. Griffith, T. M., Edwards, D. H., & Randall, M. D. Blood flow and optimal vascular topography: role of the endothelium. *Basic Res. Cardiol.* **86 Suppl 2**, 89-96 (1991).
67. Chapman, N., Haimes, G., Stanton, A.V, Thom, S. A. M., & Hughes, A. D. Acute effects of oxygen and carbon dioxide on retinal vascular network geometry in hypertensive and normotensive subjects. *Clin. Sci.* **99** (6), 483-8 (2000).
68. Heringa, S. M., Bouvy, W. H., van denBerg, E., Moll, A. C., Jaap Kappelle, L., & Jan Biessels, G. Associations between retinal microvascular changes and dementia, cognitive functioning, and brain imaging abnormalities: a systematic review. *J. Cereb. blood flow Metab.* **33** (7), 983-995 (2013).
69. Ding, J. *et al.* Diabetic retinopathy and cognitive decline in older people with type 2 diabetes: The Edinburgh type 2 diabetes study. *Diabetes.* **59** (11), 2883-2889 (2010).
70. Parisi, V., Restuccia, R., Fattapposta, F., Mina, C., Bucci, M. G., & Pierelli, F. Morphological and functional retinal impairment in Alzheimer's disease patients. *Clin. Neurophysiol.* **112** (10), 1860-1867 (2001).
71. Paquet, C., Boissonnot, M., Roger, F., Dighiero, P., Gil, R., & Hugon, J. Abnormal retinal thickness in patients with mild cognitive impairment and Alzheimer's disease. *Neurosci. Lett.* **420** (2), 97-99 (2007).
72. Moschos, M. M. *et al.* Structural and functional impairment of the retina and optic nerve in Alzheimer's disease. *Curr. Alzheimer Res.* **9** (7), 782-788 (2012).
73. Lu, Y. *et al.* Retinal nerve fiber layer structure abnormalities in early Alzheimer's disease: Evidence in optical coherence tomography. *Neurosci. Lett.* **480** (1), 69-72 (2010).
74. Kesler, A., Vakhapova, V., Korczyn, A. D., Naftaliev, E., & Neudorfer, M. Retinal thickness in patients with mild cognitive impairment and Alzheimer's disease. *Clin. Neurol. Neurosurg.* **113** (7), 523-526 (2011).
75. Ascaso, F. J. *et al.* Retinal alterations in mild cognitive impairment and Alzheimer's disease: An optical coherence tomography study. *J. Neurol.* **261** (8), 1522-1530 (2014).
76. Berisha, F., Feke, G. T., Trempe, C. L., McMeel, J. W., & Schepens, C. L. Retinal abnormalities in early Alzheimer's disease. *Investig. Ophthalmol. Vis. Sci.* **48** (5), 2285-2289 (2007).
77. Iseri P.K., Altinaş O, Tokay T, & Yüksel N. Relationship between Cognitive Impairment and Retinal Morphological and Visual Functional Abnormalities in Alzheimer Disease. *J. Neuro-Ophthalmology.* **26** (1), 18-24 (2006).
78. Garcia-Martin, E. S. *et al.* Macular thickness as a potential biomarker of mild Alzheimer's disease. *Ophthalmology.* **121** (5), 1149-1151.e3 (2014).
79. Ko, F. *et al.* Retinal Nerve Fiber Layer Thinning Associated With Poor Cognitive Function Among A Large Cohort, The Uk Biobank. *Alzheimer's Dement.* **12** (7), P317-P318 (2016).
80. Moreno-Ramos, T., Benito-Leon, J., Villarejo, A., & Bermejo-Pareja, F. Retinal nerve fiber layer thinning in dementia associated with Parkinson's disease, dementia with Lewy bodies, and Alzheimer's disease. *J. Alzheimers. Dis.* **34** (3), 659-664 (2013).
81. Moschos, M. M. *et al.* Morphologic changes and functional retinal impairment in patients with Parkinson disease without visual loss. *Eur. J. Ophthalmol.* **21** (1), 24-29 (2011).
82. Garcia-Martin, E. *et al.* Ability and reproducibility of Fourier-domain optical coherence tomography to detect retinal nerve fiber layer atrophy in Parkinson's disease. *Ophthalmology.* **119** (10), 2161-2167 (2012).
83. Yip, W. *et al.* Comparison of Common Retinal Vessel Caliber Measurement Software and a Conversion Algorithm. *Transl. Vis. Sci. Technol.* **5** (5), 11 (2016).
84. Gorelick, P. B. *et al.* Vascular contributions to cognitive impairment and dementia: a statement for healthcare professionals from the american heart association/american stroke association. *Stroke.* **42** (9), 2672-2713 (2011).

85. Brown, W. R., & Thore, C. R. Review: Cerebral microvascular pathology in ageing and neurodegeneration. *Neuropathol. Appl. Neurobiol.* **37** (1), 56-74 (2011).
86. DeSilva, T. M., & Faraci, F. M. Microvascular Dysfunction and Cognitive Impairment. *Cell. Mol. Neurobiol.* **36** (2), 241-258 (2016).
87. Kalaria, R. N., Akinyemi, R., & Ihara, M. Does vascular pathology contribute to Alzheimer changes? *J. Neurol. Sci.* **322** (1-2), 141-147 (2012).
88. Kling, M. A., Trojanowski, J. Q., Wolk, D. A., Lee, V. M. Y., & Arnold, S. E. Vascular disease and dementias: paradigm shifts to drive research in new directions. *Alzheimers. Dement.* **9** (1), 76-92 (2013).
89. O'Brien, J. T. *et al.* Vascular cognitive impairment. *Lancet Neurol.* **2** (2), 89-98 (2003).
90. Chen, C. *et al.* Alzheimer's disease with cerebrovascular disease: current status in the Asia-Pacific region. *J. Intern. Med.* **280** (4), 359-374 (2016).
91. Pérez, M. A., Bruce, B. B., Newman, N. J., & Biousse, V. The use of retinal photography in nonophthalmic settings and its potential for neurology. *Neurologist.* **18** (6), 350-5 (2012).
92. Boppart, S. A. Optical coherence tomography: Technology and applications for neuroimaging. *Psychophysiology.* **40** (4), 529-541 (2003).
93. Hee, M. R. *et al.* Optical coherence tomography of the human retina. *Arch. Ophthalmol.* **113** (3), 325-32 (1995).
94. Huang, D. *et al.* Optical coherence tomography. *Science (80-.).* **254** (5035), 1178-81 (1991).
95. vanVelthoven, M. E. J., Verbraak, F. D., Yannuzzi, L., Rosen, R. B., Podoleanu, A. G. H., &deSmet, M. D. Imaging the retina by en face optical coherence tomography. *Retina.* **26** (2), 129-136 (2006).
96. Costa, R. A. *et al.* Retinal assessment using optical coherence tomography. *Prog. Retin. Eye Res.* **25** (3), 325-353 (2006).
97. DeBuc, D. C., Somfai, G. M., Ranganathan, S., Tátrai, E., Ferencz, M., &Puliafito, C. A. Reliability and reproducibility of macular segmentation using a custom-built optical coherence tomography retinal image analysis software. *J. Biomed. Opt.* **14** (6), 64023 (2009).
98. Budenz, D. L. *et al.* Determinants of Normal Retinal Nerve Fiber Layer Thickness Measured by Stratus OCT. *Ophthalmology.* **114** (6), 1046-1052 (2007).
99. Leung, C. K. S. *et al.* Retinal Nerve Fiber Layer Imaging with Spectral-Domain Optical Coherence Tomography: A Prospective Analysis of Age-Related Loss. *Ophthalmology.* **119** (4), 731-737 (2012).
100. Cettomai, D. *et al.* Reproducibility of optical coherence tomography in multiple sclerosis. *Arch. Neurol.* **65** (9), 1218-1222 (2008).
101. Garcia-Martin, E., Pinilla, I., Idoipe, M., Fuertes, I., & Pueyo, V. Intra and interoperator reproducibility of retinal nerve fibre and macular thickness measurements using Cirrus Fourier-domain OCT. *Acta Ophthalmol.* **89** (1) (2011).
102. Garcia-Martin, E., Pueyo, V., Pinilla, I., Ara, J.-R., Martin, J., & Fernandez, J. Fourier-domain OCT in multiple sclerosis patients: reproducibility and ability to detect retinal nerve fiber layer atrophy. *Invest. Ophthalmol. Vis. Sci.* **52** (7), 4124-31 (2011).
103. Menke, M. N., Knecht, P., Sturm, V., Dabov, S., & Funk, J. Reproducibility of nerve fiber layer thickness measurements using 3D fourier-domain OCT. *Invest. Ophthalmol. Vis. Sci.* **49** (12), 5386-91 (2008).
104. Mwanza, J. C. *et al.* Reproducibility of peripapillary retinal nerve fiber layer thickness and optic nerve head parameters measured with cirrus HD-OCT in glaucomatous eyes. *Investig. Ophthalmol. Vis. Sci.* **51** (11), 5724-5730 (2010).
105. Syc, S. B. *et al.* Reproducibility of high-resolution optical coherence tomography in multiple sclerosis. *Mult Scler.* **16** (7), 829-839 (2010).
106. Ikram, M. K., Cheung, C. Y., Wong, T. Y., & Chen, C. P. L. H. Retinal pathology as biomarker for cognitive impairment and Alzheimer's disease. *J. Neurol. Neurosurg. Psychiatry.* **83** (9), 917-22 (2012).
107. MacGillivray, T. J., Trucco, E., Cameron, J. R., Dhillon, B., Houston, J. G., & vanBeek, E. J. R. Retinal imaging as a source of biomarkers for diagnosis, characterization and prognosis of chronic illness or long-term conditions. *Br. J. Radiol.* **87** (1040), 20130832 (2014).
108. Patton, N. *et al.* Retinal image analysis: Concepts, applications and potential. *Prog. Retin. Eye Res.* **25** (1), 99-127 (2006).
109. McGrory, S. *et al.* The application of retinal fundus camera imaging in dementia: A systematic review. *Alzheimer's Dement. Diagnosis, Assess. Dis. Monit.* **6**, 91-107 (2017).
110. Wong, T. Y., Knudtson, M. D., Klein, R., Klein, B. E. K., Meuer, S. M., & Hubbard, L. D. Computer-assisted measurement of retinal vessel diameters in the Beaver Dam Eye Study: methodology, correlation between eyes, and effect of refractive errors. *Ophthalmology.* **111** (6), 1183-90 (2004).
111. Hardin, J. S., Taibbi, G., Nelson, S. C., Chao, D., & Vizzeri, G. Factors Affecting Cirrus-HD OCT Optic Disc Scan Quality: A Review with Case Examples. *J. Ophthalmol.* **2015**, 1-16 (2015).
112. Kim, N. R. *et al.* Influence of Cataract on Time Domain and Spectral Domain Optical Coherence Tomography Retinal Nerve Fiber Layer Measurements. *J. Glaucoma.* , 1 (2010).
113. Li, H. *et al.* Lens opacity and refractive influences on the measurement of retinal vascular fractal dimension. *Acta Ophthalmol.* **88** (6), e234-e240 (2010).
114. Maberley, D., Morris, A., Hay, D., Chang, A., Hall, L., & Mandava, N. A comparison of digital retinal image quality among photographers with different levels of training using a non-mydriatic fundus camera. *Ophthalmic Epidemiol.* **11** (3), 191-7 (2004).
115. Rochtchina, E., Wang, J. J., Taylor, B., Wong, T. Y., & Mitchell, P. Ethnic variability in retinal vessel caliber: A potential source of measurement error from ocular pigmentation?-The Sydney childhood eye study. *Investig. Ophthalmol. Vis. Sci.* **49** (4), 1362-1366 (2008).
116. Wainwright, A. *et al.* Effect of image quality, color, and format on the measurement of retinal vascular fractal dimension. *Investig. Ophthalmol. Vis. Sci.* **51** (11), 5525-5529 (2010).
117. Nguyen, T. T., & Wong, T. Y. Retinal vascular manifestations of metabolic disorders. *Trends Endocrinol. Metab.* **17** (7), 262-268 (2006).
118. Ding, J. *et al.* Retinal vascular caliber and the development of hypertension: a meta-analysis of individual participant data. *J. Hypertens.* **32** (2), 207-15 (2014).
119. Nguyen, T. T., & Wong, T. Y. Retinal vascular changes and diabetic retinopathy. *Curr. Diab. Rep.* **9** (4), 277-283 (2009).
120. Leung, C. K. S., Ye, C., Weinreb, R. N., Yu, M., Lai, G., & Lam, D. S. Impact of Age-related Change of Retinal Nerve Fiber Layer and Macular Thicknesses on Evaluation of Glaucoma Progression. *Ophthalmology.* **120** (12), 2485-2492 (2013).
121. Sherry, L. M. *et al.* Reliability of computer-assisted retinal vessel measurement in a population. *Clin. Experiment. Ophthalmol.* **30** (3), 179-182 (2002).
122. Wardlaw, J. M. *et al.* Neuroimaging standards for research into small vessel disease and its contribution to ageing and neurodegeneration. *Lancet Neurol.* **12** (8), 822-838 (2013).
123. Patton, N., Aslam, T., MacGillivray, T., Pattie, A., Deary, I. J., & Dhillon, B. Retinal vascular image analysis as a potential screening tool for cerebrovascular disease: A rationale based on homology between cerebral and retinal microvasculatures. *J. Anat.* **206** (4), 319-348 (2005).
124. Ferri, C. P. *et al.* Global prevalence of dementia: A Delphi consensus study. *Lancet.* **366** (9503), 2112-2117 (2005).
125. Sahadevan, S. *et al.* Ethnic differences in Singapore's dementia prevalence: The stroke, Parkinson's disease, epilepsy, and dementia in Singapore study. *J. Am. Geriatr. Soc.* **56** (11), 2061-2068 (2008).

126. Kernt, M. *et al.* Assessment of diabetic retinopathy using nonmydriatic ultra-widefield scanning laser ophthalmoscopy (Optomap) compared with ETDRS 7-field stereo photography. *Diabetes Care.* **35** (12), 2459-2463 (2012).
127. Manivannan, A., Plskova, J., Farrow, A., Mckay, S., Sharp, P. F., &Forrester, J.V. Ultra-wide-field fluorescein angiography of the ocular fundus. *Am. J. Ophthalmol.* **140** (3), 525-527 (2005).
128. Pellegrini, E. et al. Blood vessel segmentation and width estimation in ultra-wide field scanning laser ophthalmoscopy. *Biomed. Opt. Express.* **5** (12), 4329 (2014).
129. Estrada, R., Tomasi, C., Schmidler, S. C., & Farsiu, S. Tree topology estimation. *IEEE Trans. Pattern Anal. Mach. Intell.* **37** (8), 1688-1701 (2015).

